AD 404 504

AFCRL-63-87
APRIL 1963

63-3-4

Research Report

High Altitude X-Band Noise Measurements

S. HUNT
A. S. ORANGE
K. GLICK

COMMUNICATIONS SCIENCES LABORATORY PROJECT 4610
AIR FORCE CAMBRIDGE RESEARCH LABORATORIES, OFFICE OF AEROSPACE RESEARCH, UNITED STATES AIR FORCE, L.G. HANSCOM FIELD, MASS.

Requests for additional copies by Agencies of the Department of Defense, their contractors, and other government agencies should be directed to the:

Armed Services Technical Information Agency
Arlington Hall Station
Arlington 12, Virginia

Department of Defense contractors must be established for ASTIA services, or have their 'need-to-know' certified by the cognizant military agency of their project or contract.

All other persons and organizations should apply to the:

U. S. DEPARTMENT OF COMMERCE
OFFICE OF TECHNICAL SERVICES,
WASHINGTON 25, D. C.

AFCRL-63-87
APRIL 1963

Research Report

High Altitude X-Band Noise Measurements

S. HUNT
A. S. ORANGE
K. GLICK

COMMUNICATIONS SCIENCES LABORATORY PROJECT 4610
AIR FORCE CAMBRIDGE RESEARCH LABORATORIES, OFFICE OF AEROSPACE RESEARCH, UNITED STATES AIR FORCE, L.G. HANSCOM FIELD, MASS.

Abstract

X-band noise temperature data obtained with an airborne radiometer installed in a high-speed jet aircraft (KC-135) is presented. The aircraft was found to be an electrically quiet environment at X-band. The data shows the considerable influence of blackbody radiation from the earth entering the antenna sidelobes. Temperatures close to those calculated theoretically were measured over water and at high antenna elevation angles. Heavy clouds, though many thousands of feet below the aircraft, caused a considerable temperature increase. A trend of lower temperatures with increasing altitude was observed. The apparent temperatures of land, snow, and ice and water is discussed.

Acknowledgments

The authors acknowledge the cooperation of the Air Force flight and ground-support personnel. Their skill in operating and maintaining the aircraft contributed greatly to the success of this experiment.

Contents

Illustrations

High Altitude X-Band Noise Measurements

1. INTRODUCTION

The advent of low-noise devices and techniques and high-power transmitting equipment at X-band frequencies has led to increased consideration of X-band systems for reliable long-range communication. Extension of system concepts to include an airborne terminal offers a potential solution to the air-ground-air communication problem. However there has been little or no data available concerning the noise environment of high-altitude, high-speed, jet aircraft.

This report presents a summary of data gathered using an X-band radiometer in an experiment conducted from September through December 1961 by the Communication Sciences Laboratory, of the Air Force Cambridge Research Laboratories.

2. DESCRIPTION OF EXPERIMENT

The experiment was conducted using a comparison radiometer installed in an Air Force KC-135 jet tanker aircraft. Figure 1 shows a block diagram of the radiometer, and Appendix A contains a description of system operation. The radiometer had a sensitivity range from $2^{\circ}K$ to room temperature, with an accuracy of $\pm 4^{\circ}K$ over this range with a 4-sec integration time. The radiometer was a double-sideband,

(Authors' manuscript received for publication 9 January 1963)

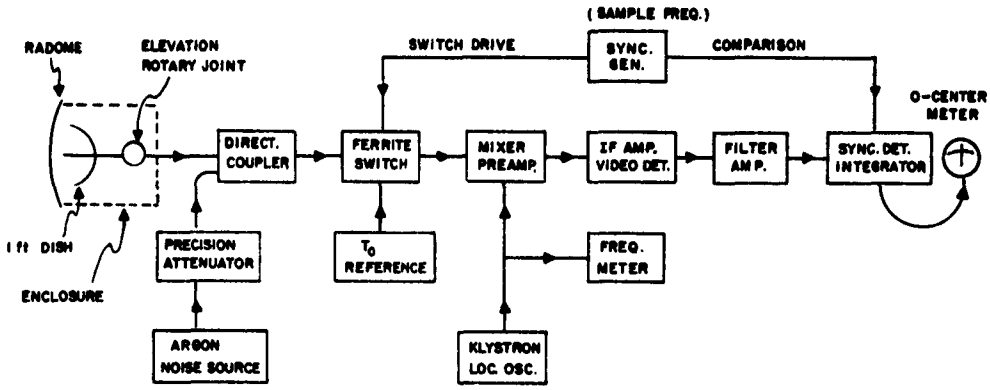

Figure 1. Radiometer Block Diagram

single conversion, null balance, room temperature reference comparison device. Center frequency (klystron frequency) was 8050 Mcps, followed by a 30 Mcps IF amplifier with 10 Mcps bandwidth. The system was built to airborne specifications. With the exception of local oscillator, argon noise source, IF preamplifier and amplifier, the device was of solid-state construction, designed and built by laboratory personnel.

The antenna was a horizontally-polarized parabolic dish measuring 1 ft in diameter. It was located on the right side of the KC-135, forward of the wing and engine nacelles, and mounted inside the fuselage behind a 0.7 inch thick laminated fiberglass radome installed flush with the aircraft skin. The antenna was scanned in elevation from 5° below to 20° above aircraft horizontal; and, with a $\pm 30^{\circ}$ bank by the aircraft a total elevation coverage from -35° to $+50^{\circ}$ could be obtained. This report references all antenna elevation angles to the aircraft horizontal; that is, a zenith angle of 90°. However it must be remembered that at 34,000 ft altitude, the optical horizon lies 3° below aircraft horizontal. The antenna was fixed in azimuth perpendicular to the direction of flight. Except for the radome, the dish was completely enclosed on all sides and shielded from spurious signals originating within the aircraft. Figures 2 and 3 are photographs of the antenna and radome installation.

Antenna patterns were obtained with the antenna within its enclosure with and without the radome. Rough measurements were made with the antenna installed in the aircraft to check gross beam distortion. The installed antenna system had a beamwidth of 8° and a sidelobe level approximately 25 db down from the main beam. Antenna patterns are displayed and discussed in Appendix C. Changes in elevation angle created 10 to 20 percent beam broadening at certain elevations; but this factor was not considered in data reduction. Radome loss and reradiated energy were very strongly dependent on elevation angle, and a suitable correction factor was

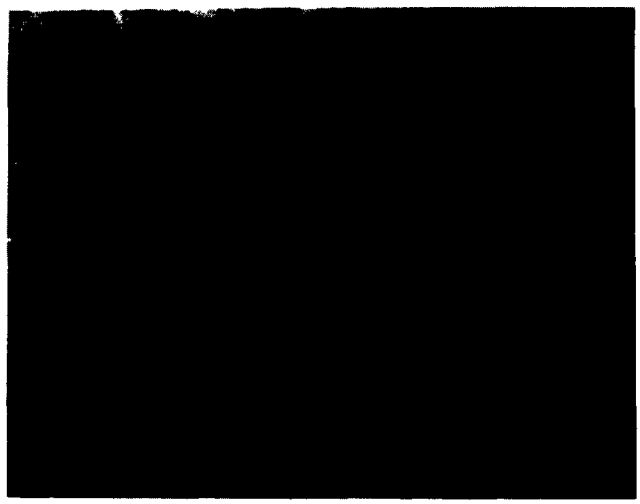

Figure 2. Radiometer Rack and Antenna Enclosure (upper left center)

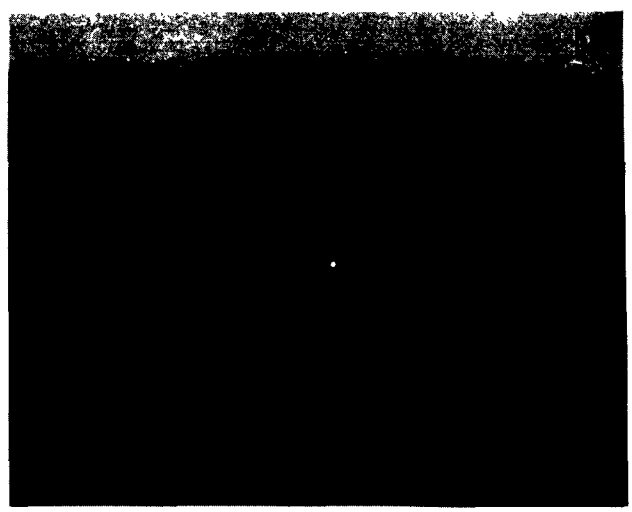

Figure 3. Radome (large arrow) and Observation Window (small arrow)

determined and applied to the data. This procedure is discussed in Appendix B. All measurements were made using horizontal polarization.

Information that included null balance reading, antenna elevation angle, reference load temperature, aircraft skin temperature, and aircraft position and heading was provided to the operator. Operation consisted of balancing the radiometer and noting the attenuation setting for balance along with the other information. From this data and the correction factors discussed in Appendix B, the source temperature was calculated. An observation window was provided the operator for visual correlation of the data with external environment.

Data-gathering flights were conducted to determine both the effect, if any, of the aircraft environment at X-band and the noise temperature observed under conditions of varying aircraft altitude, meteorological conditions, and terrain.

Seven local flights in the vicinity of L.G. Hanscom Field, Bedford, Massachusetts, were flown between September and December 1961. Two long-distance missions were accomplished: one to the Far North in early November and the other to the Caribbean area in early December, 1961. The purpose of these two flights was to study terrain temperatures and meteorological effects not available in the local areas.

The local flights served to familiarize personnel with the system and its limitations, provided aircraft noise environment data, and provided information for approximate radome loss definition, antenna sidelobe response, noise temperature as a function of altitude and antenna elevation, and weather and terrain effects during the fall-to-winter seasonal change from foliage to snow in the Bedford area.

The Far North mission covered a route from Bedford northerly to Frobisher Bay (Baffin Island), west along the 65th parallel to a landing at Anchorage, Alaska, south to a landing at Travis AFB, California, and east to Bedford. This route provided data in the polar region, in the North Pacific area, and through the middle latitudes of the United States. Terrain along this route consisted of snow, water, various foliage types, dry plains, desert, and farmland.

The Caribbean mission followed an over-water path south to Ramey AFB, Puerto Rico, and return. There were three flights from Puerto Rico: two in the local area, and one proceeding along the South American coast to the equator, then east several hundred miles toward Africa, and finally northwest to Ramey AFB. This mission provided over-water data near the equator, as well as data on cloud effects.

The data to be presented has been corrected to a first approximation for radome losses and reradiation (see Appendix B). However, because of insufficient documentation of antenna patterns with the antennas installed in the aircraft, no analytic attempt has been made to remove the effects of sidelobe contributions from external sources.

3. RESULTS

Presentation of results is divided into six categories: Aircraft Noise Environment; Near-Horizontal-Elevation Angle Noise Temperatures; Observed Temperature Variations as Functions of Terrain; Noise Temperature as a Function of Altitude and Antenna Elevation; Cloud Studies; and Miscellaneous Studies.

3.1 Aircraft Noise Environment

One goal of the experimental program was to determine whether the aircraft itself acted as a noise source. A secondary consideration was interference from normal operation of aircraft electrical and electronic equipment.

Early in the flight program a series of tests of noise temperature levels and interference was conducted. These tests were repeated occasionally in later flights, and observations of any unusual system responses were made on all flights. Aircraft speed and engine power settings were varied over the complete operational range and the background noise was noted from the radiometer. All aircraft radio, navigation, and electrical equipment was turned on and off in a search for possible interference. These tests failed to produce measurable variations in observed noise temperature. At no time during normal data-gathering operations were anomalies in response noted which could be traced to aircraft-generated interference. It has been concluded that, within the sensitivity of the radiometer, neither the aircraft moving through the air nor any of the equipment on board contributed to the noise temperature measured. It should be noted that a complete statement on aircraft effects would require observing the engine exhaust.

3.2 Near-Horizontal Elevation Angle Noise Temperatures

Data was obtained with the aircraft in level flight at altitudes from 32,000 to 35,000 ft. Unless otherwise noted, meteorological conditions were such that clouds at worst were scattered-to-broken at or below 10,000 ft, with no more than light cirrus cover at or above aircraft altitude. These conditions appeared to have no effect on the data in this section. Included observation angles varied from -5° to $+20^{\circ}$ with respect to level flight. Generally, data points were taken at 3° elevation angle increments from $+20^{\circ}$ to -1°, with a final -5° reading. At one time or another, all included angles were sampled in 1° increments.

Early in the experiment the discovery was made that, due to inclusion of the earth in the antenna sidelobes, the type of terrain overflown (that is, apparent terrain temperature) had a large influence on measured temperature at all antenna angles.

This effect and its implications in data interpretation are discussed in detail in Section 3.3. The effect permits organization of the data into three groupings independent of geographical location: that obtained over water, snow, and land.

3.2.1 OVER WATER DATA

Figure 4 displays data taken over water, primarily from the Caribbean mission. Curve A is from the Far North mission and describes readings taken over the Pacific between Alaska and California. Curves B, C, and D are taken from the equatorial flight portion of the Caribbean mission; and Curve E shows data taken on the return to Bedford from the Caribbean. Due to low apparent water noise temperature, these values are the lowest obtained in the experiment. The temperatures shown for an antenna elevation angle of 20° (2° to 7°K) are what one would expect to observe within the accuracy of the radiometer. At lower elevation angles sidelobe energy becomes important and only an upper limit on realizable noise temperatures can be obtained. Apparent sidelobe contribution can be noted from a comparison of the data with a theoretical curve (Figure 7).

3.2.2 OVER LAND DATA

Figure 5 is a plot of noise temperature as a function of antenna elevation angle for four sets of over-land data. Curve A is from samples of early local flights. Curves B and C are from data obtained in Northern Maine and Southern Canada, while Curve D represents data obtained near Travis AFB in the California-Nevada area.

Curves A, B, and C are all from data taken over land that was partially to mostly green, and Curve D is from data taken over broken hills and flat bare plains. A comparison of this data with that obtained over water (Figure 4) shows the considerable increase in temperatures measured over land over those measured over water. This apparently is due to sidelobe pick-up of radiation from the earth below, even at high antenna elevation angles. In examining Figure 5 one should keep in mind that the data does not represent sky temperature but rather an upper limit on temperatures to be observed over land with an antenna system such as the one used for this experiment.

3.2.3 OVER SNOW DATA

Figure 6 shows data taken over varying amounts of snow cover. Curves A, B, C, and D derive from data obtained between Bedford and Alaska. There was some ground fog and undercast observed up to 10,000 ft for A and B. Observations indicated that there was a higher and very thick undercast during observations corresponding to Curve C. Curve D derives from near Travis AFB, California, on return to Bedford while over snow-covered mountains and hills. Curve E is a plot of one set of observations taken at night on a local flight in December. This data

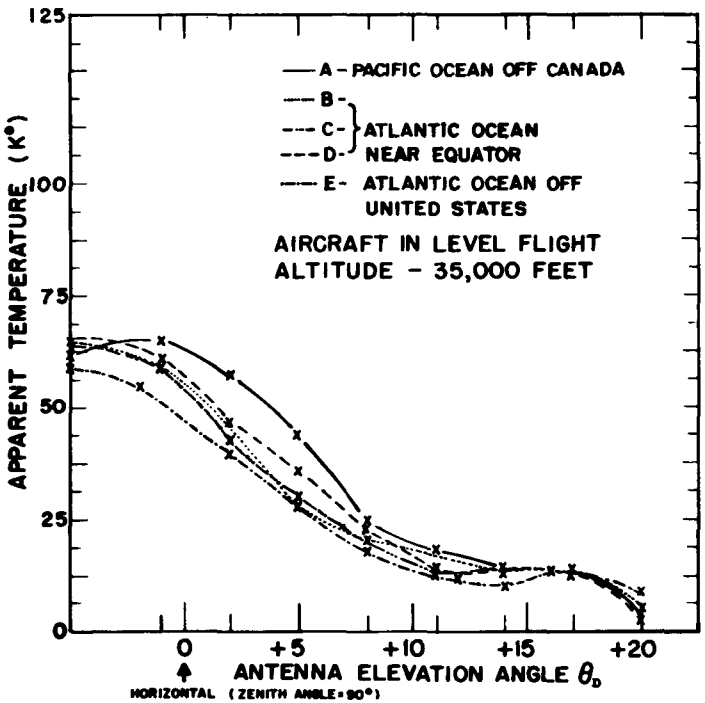

Figure 4. Curves of Data taken Over Water

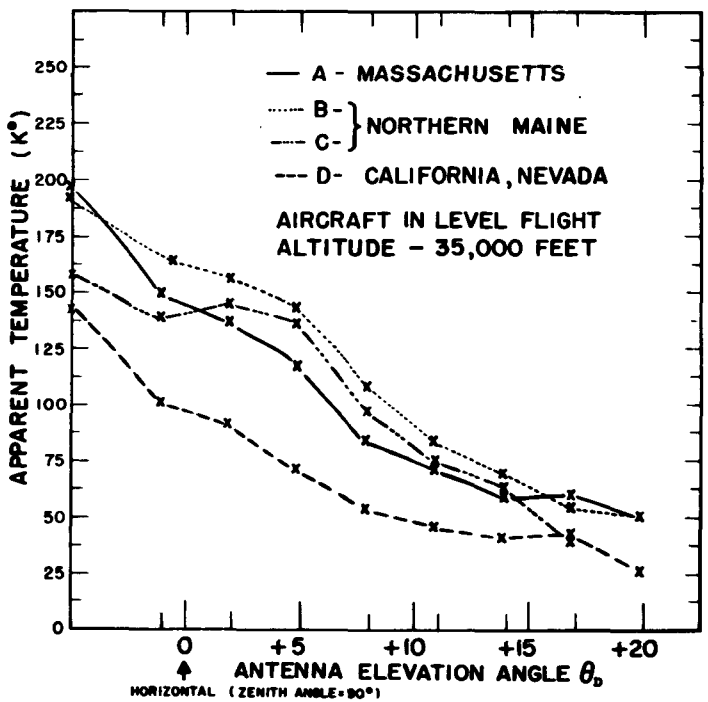

Figure 5. Curves of Data taken Over Land

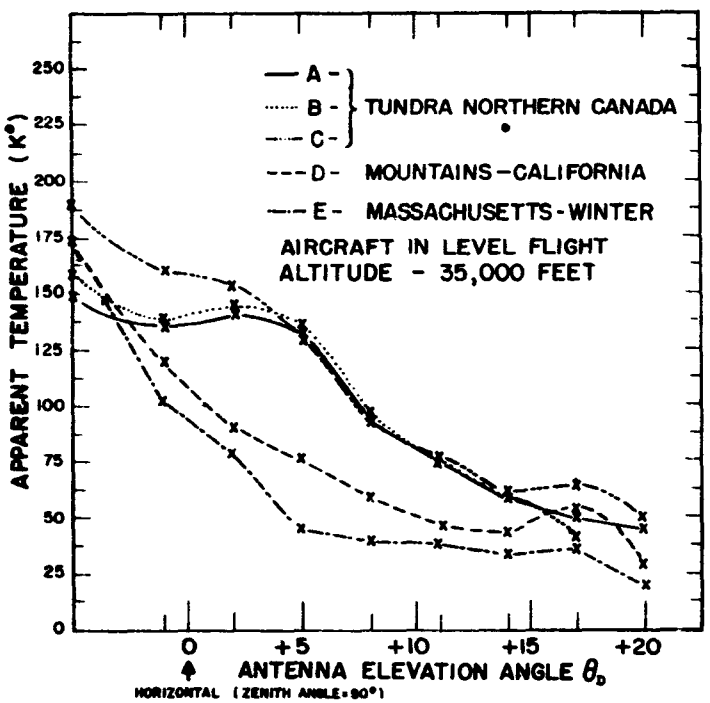

Figure 6. Curves of Data taken Over Snow

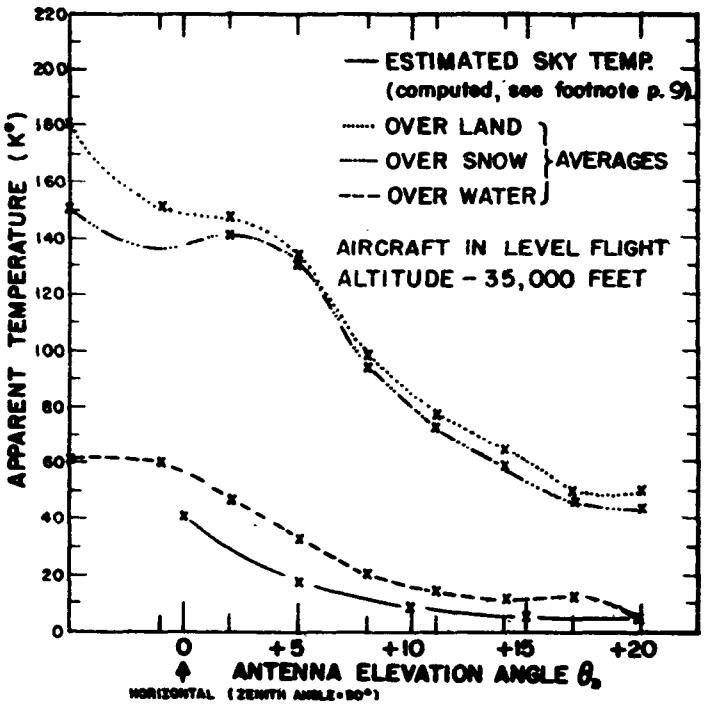

Figure 7. Comparison of Over-Water, Over-Land, and Over-Snow Data

is seen to be not vastly different from that obtained over land.

Figure 7 summarizes the above data, presenting along with calculated values* the average temperatures obtained at 35,000 ft altitude over land, water, and snow.

3.3 Observed Temperature Variations as Functions of Terrain

Noise temperature characteristics of diverse ground environments were sampled by banking the aircraft 30° to the right from horizontal. This pointed the antenna at the ground and allowed data collection at an antenna elevation angle 35° below the horizontal.

Table 1 summarizes indicated source temperature as a function of ground environment. The data were obtained from flights at various altitudes over diverse terrain. Entries 2 and 3 of Table 1 illustrate the effect of small amounts of land within the antenna sidelobes. Note that the temperatures observed in the three categories—over water, land, and snow—are consistent from place to place.

3.4 Noise Temperature as a Function of Altitude and Antenna Elevation

Several attempts were made to measure the variation of noise temperature with altitude; and Figure 8 presents data obtained on one representative flight. The data plotted together in Figure 8 were obtained with the antenna pointing at the same azimuth angle. Data of this type are extremely difficult to analyze because of the varying effects of ground reradiation and distant clouds. At all antenna elevation angles a trend of lower temperatures with greater altitude was noted. The effect varied from a few degrees Kelvin over a variation in altitude of 30,000 ft at a high antenna elevation angle (20°) to 40°K looking horizontally.

3.5 Cloud Studies

During the flights, care was taken to record cloud conditions for correlation with noise data. Inspection of these records and their correlation with observed noise temperature allowed definition of normal or average meteorological conditions, that is, conditions of clouding which contributed no measurable noise temperature in the data gathering. These conditions were: clouds no heavier than scattered-to-broken and no higher than 10,000 ft; no more than light cirrus above aircraft altitude;

*A. Andermann, L. L. Oh, and C. D. Lunden "Design Study for Experimental Airborne Antenna for KC-135 Aircraft," AF Contract No. AF19(604)-7373, Boeing Aircraft Co., Transport Division, Renton, Wash.

TABLE 1. Summary of Indicated Source Temperature as a Function of Ground Environment

(a) Over-Water Data at -35° Antenna Elevation Angle

Temp °K	Altitude $\times 10^3$ ft	Location	Remarks
106	5	Bedford local	
133	5	Bedford local	Land in sidelobes
155	5	Bedford local	Land in sidelobes
88	25	Caribbean	Massachusetts—Puerto Rico
87	35	Caribbean	Massachusetts—Puerto Rico
86	30	Caribbean	Equatorial flight
96	34	Caribbean	Land mass to right
92	34	Caribbean	Equatorial average of 4
86	32	Caribbean	Equatorial average of 2
80	35	Caribbean	Puerto Rico—Massachusetts
80	17	Bedford local	Night
80	8.5	Bedford local	Night, average of 9

	(b) Over-Land Data at -35° Antenna Elevation Angle		
266	33	Bedford local	Scattered clouds to 10,000 ft
272	35	Bedford local	Scattered clouds to 10,000 ft
271	5	Bedford local	Blue Hills, Massachusetts
294	5	Bedford local	Wooded area, Massachusetts
>293	5	Bedford local	Blue Hills, Massachusetts, haze
252	35	Far North	Thin cloud cover 10,000–12,000 ft
226	33	United States	California—Massachusetts, average of 6
146	33	United States	Bonneville Salt Flats, Utah
233	33	United States	Flat plain—Central U.S.
240	33	United States	Farmland—Central U.S.
248	26	Puerto Rico	

	(c) Over-Snow Data at -35° Antenna Elevation Angle		
241	35	Far North	Maine—Alaska, average of 5
241	33	Far North	California area snow-covered hills
228	33	Far North	California area uniform snow
229	33	Far North	California area heavy snow basin
231	30	Bedford local	Night, snow-covered fields
230	35	Bedford local	Night, snow covered fields
223	29-11	Bedford local	Night, snow-covered fields Average of 7, no altitude effects
235	5	Bedford local	Night, snow-covered fields Banked turn average of 8

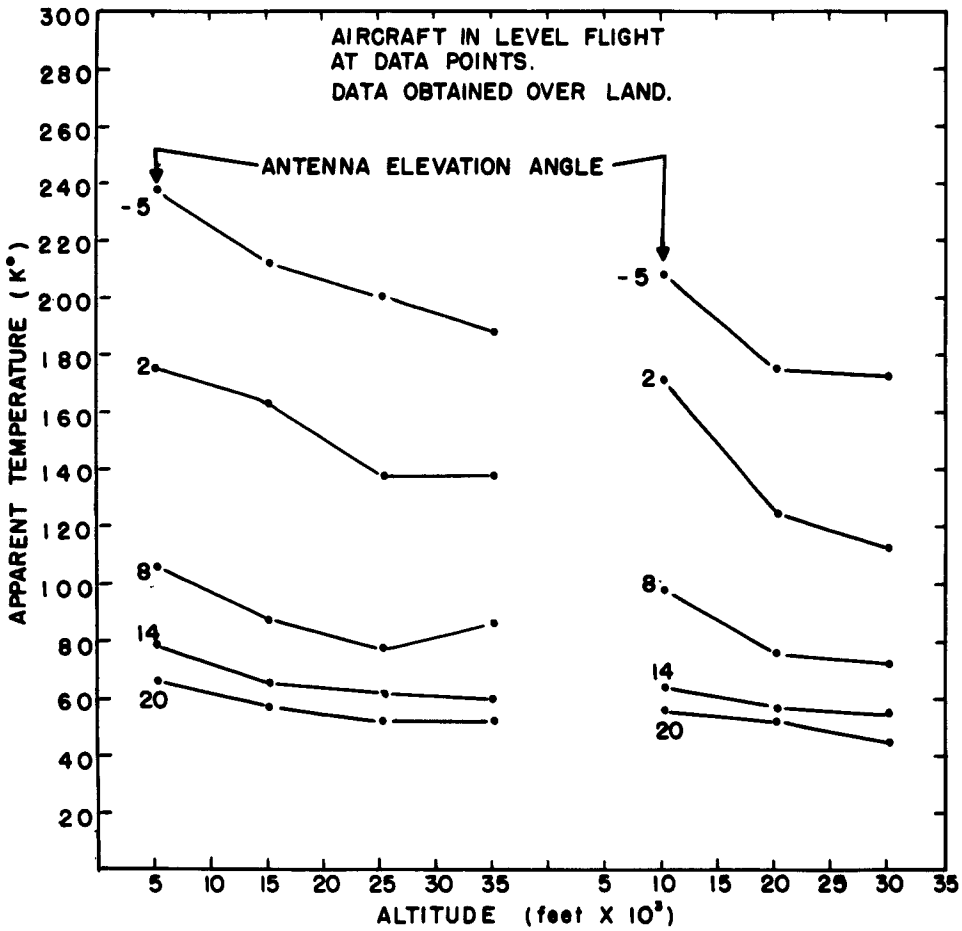

Figure 8. Temperature Variation with Altitude

and no more than moderately hazy conditions. Any heavier cloud formations are the subject of this section.

Any clouds containing a great deal of moisture extending more than a few thousand feet above the ground contribute noise energy to the antenna through its sidelobes. An example would be heavy altostratus formations. Even clouds with moderate moisture content, such as cumulus, in or near the main beam of the antenna contribute markedly to received energy. Cumulonimbus clouds, occurring at or above 10,000 ft altitude, produce very noticeable increases in observed noise temperature.

Figures 9, 10, and 11 indicate data obtained when cloud cover was more severe than the above-noted average conditions over water, land, and snow. Each figure also contains a noise temperature reference curve which represents the data average under average conditions for that type of terrain. These figures are based on data recorded at altitudes near 35,000 ft.

Figure 9 shows effects of a medium density cloud layer at flight altitude over land on a local flight. Temperature increases of as much as 60° were noted, with the average increase about 20°. The cloud curves are shown in straight-line segments as each curve represents only one set of data points.

Figure 10 demonstrates the effects of cloud contributions over snow observed from a flight altitude of 35,000 ft along the 65th parallel on the Far North mission. All three curves were taken while flying over heavy altostratus which appeared to be at an altitude of 10,000 ft. There also were scattered cirrus below the aircraft. Each curve again represents one set of measurements. The altostratus caused considerable temperature increases at near-horizontal antenna elevation angles. The high elevation angle increase was due either to cirrus above flight altitude or sidelobe pickup at the lower clouds.

Figure 11 illustrates effects noted over water. Curves 1A and 1B derive from the Alaska-to-California leg of the Far North mission. Aircraft altitude was 35,000ft and there was a thick undercast at an unknown altitude. Curves 1A and 1B are each taken from one set of observations. Curves 2, 3, and 4 are from the Caribbean mission. Curve 2 represents the average of five sets of measurements made at 25,000 ft altitude on the Massachusetts-to-Puerto Rico leg of the mission. Moderate altostratus formations were observable at about 7000 ft in the distance, and haze was moderate. Curves 3 and 4 are from the equatorial flight. Curve 3 represents the average of four sets of observations at altitudes between 30,000 and 34,000 ft. There was a broken undercast to 15,000 ft, with some scattered cumulonimbus extending much higher in the distance. Curve 4 represents the average of three groups of observations of the distant land mass and heavy cloud banks up to aircraft altitude of 34,000 ft. The data obtained over a solid undercast (Curves 1A and 1B) show a considerable temperature enhancement at all antenna elevation angles.

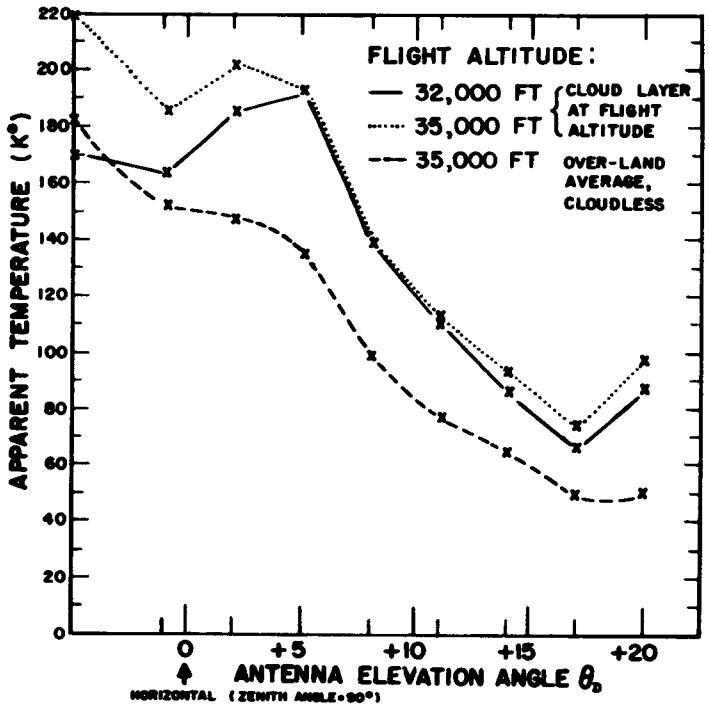

Figure 9. Effects of Medium Density Cloud Cover Over Land

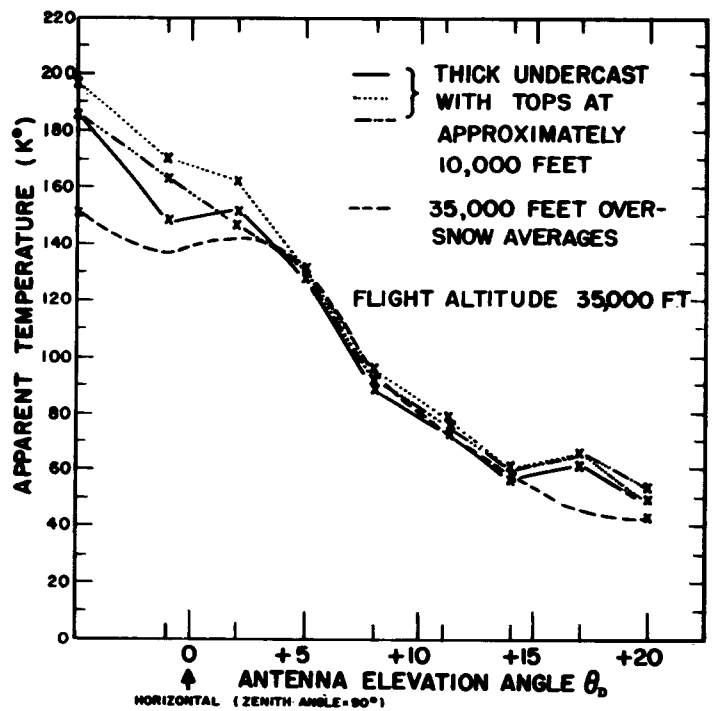

Figure 10. Effects of Cloud Contributions Over Snow

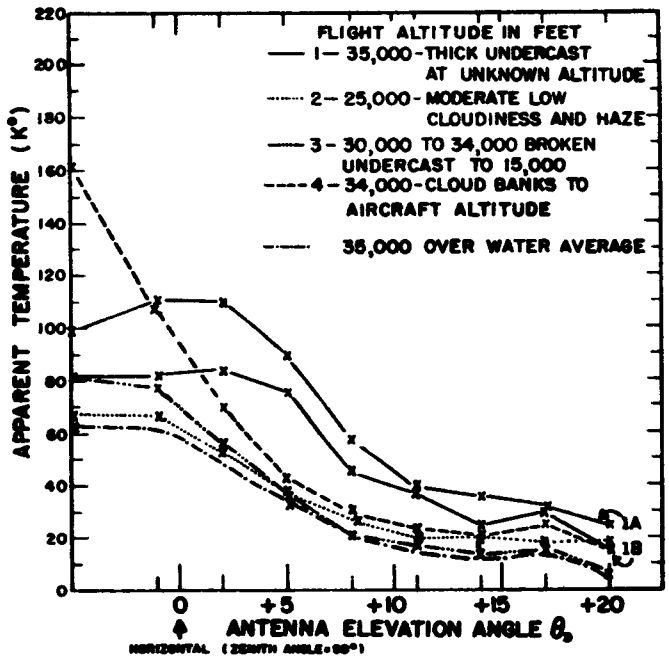

Figure 11. Effects of Cloud Contributions Over Water

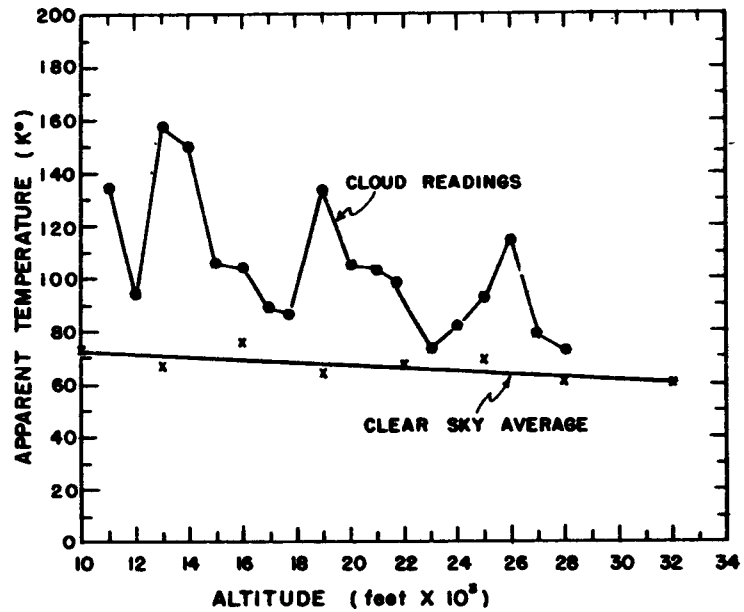

Figure 12. Observed Noise Temperature as a Function of Altitude within Cloud Buildups

Broken clouds decks appear to have little effect on the data. Cloud banks at aircraft altitude (Curve 4) causes the largest temperature increase at near-horizontal elevation angles.

During the Caribbean mission, attempts were made to catalog observed noise temperature (and thus vapor density) as a function of altitude within cloud buildups. Figure 12 is a plot of the data from one such study. However this data may have been compromised by land contamination in the background, since it was obtained by flying a polygonal pattern around the cloud buildup, each side of the polygon being 1000 ft lower than the preceding one.

Other attempts were even more inconclusive because the cloud buildups were few and of short lifetime (about 20 minutes from start to dispersion).

The radiometer was operated while the aircraft was flying through heavy clouds. Temperature variations were so great and rapid that a quantitive statement cannot be made regarding observed temperatures other than to note that their magnitudes were considerably larger than when the clouds were not present.

3.6 Miscellaneous Studies

Before data flights began there was not sufficient time to define the effect of antenna enclosure and radome upon the antenna pattern. Since the radome could not be removed from the aircraft mounting because of repressurization problems, a technique was evolved to establish 'ballpark' characteristics of the antenna system during data flights (see Appendix B for derivation and description). This 'window profile' technique yielded data for elevation angles up to 40° above horizontal. That data and additional data taken up to 70° above the horizontal form the basis of Table 2.

TABLE 2. Average Temperatures as Functions of Terrain and Elevation Angle

Antenna Elevation Angle		$+30^{\circ}$	$+40^{\circ}$	$+50^{\circ}$	$+70^{\circ}$
Observed Temperature	Over Land	$34^{\circ}K$	$27^{\circ}K$	$21^{\circ}K$	$15^{\circ}K$
	Over Water	$4^{\circ}K$	$3^{\circ}K$	$0^{\circ}K$	—
	Over Snow	$15^{\circ}K$	$22^{\circ}K$	$17^{\circ}K$	—

Land and water values are averages of a minimum of eight samples per angle. The snow averages, however, represent at most only three samples per angle. There were no samples taken at 70° above horizontal for either snow or water. At near-zenith elevation angles the influence of the earth became negligible, even when flying over land.

Early local flights covered environment response for frequencies of 7750 and 8350 Mcps, as well as 8050 Mcps. Since no unusual responses as a function of

radiometer frequency were observed, and since there was no information on antenna patterns at upper and lower frequencies, all remaining tests were conducted at 8050 Mcps.

Two flights gave information regarding auroral phenomena, although it was not expected that the aurora would be an X-band noise source. In each case, the aurora was a curtain parallel to the line of flight, over 100 miles distant, covering about a 3° angle in elevation, and centered at an observation angle of -2° with respect to horizontal. Five minutes of observation by scanning the antenna through the curtain elevation angles failed to produce measurable differences from clear sky readings.

4. CONCLUSIONS

4.1 General Conclusions

In drawing conclusions concerning high-altitude X-band noise temperatures from the data, certain statements may be made assuming nothing more than time-invariant measurement system parameters.

(1) At an antenna location on the right side of the aircraft forward of the wing, no aircraft interference or aircraft-environment effects could be detected. This conclusion, however, cannot be considered valid necessarily for antenna locations that would allow observation through engine exhausts.

(2) Medium-to-heavy cloud cover above 10,000 ft can add as much as 60°K to observed noise temperature for an aircraft altitude of approximately 35,000 ft. If this cloud cover lies in the main beam of the antenna, considerable noise fluctuations will be observed.

(3) Considering ground environments of land, snow, and water separately, no significant correlation between observed noise temperature and geographical location existed. For example, data taken over land gave the same average temperature regardless of geographical location.

4.2 Derivational Conclusions

Results of tests performed during project missions and on the antenna-enclosure-radome complex after removal from the aircraft indicate a noticeable effect of the antenna enclosure and radome upon the beam structure of the antenna as a function of antenna elevation angle.

The conclusion that sidelobe energy pickup accounts for the disparities shown in Figure 7 (page 8) is inescapable. Tests were performed near land-water interfaces.

For example the aircraft was flown over water toward land on a course perpendicular to the land-water boundary. As the aircraft approached the vicinity of the shoreline, observed noise temperatures would start rising from average over-water values and would reach average over-land values very shortly after the aircraft passed inland. Indeed, it was not even necessary to observe the ground environment because the change in observed noise was so rapid and consistent that the operator could predict and determine shoreline crossings.

As a further support for this conclusion, extensive pattern tests were performed on the antenna complex after completion of airborne work. The antenna, enclosure, radome, and a sheet of aluminum (to simulate the aircraft skin at the edges of the radome) were placed on an antenna range. Rough three-dimensional patterns as a function of elevation angle were taken. On the basis of these patterns, estimates of noise energy entering the antenna from land equivalent to a blackbody radiator were made. Subtraction of the estimated energy as a function of elevation angle from the over-land average noise curve brought the resultant curve into close agreement with the over-water noise average.

Examination of the average values of noise observed over land, over water, and over snow at elevation angles of -35° and -5° (with respect to the horizontal) are of interest. These values are shown in Table 3. It is noted that land has the expected indicated ambient temperature at -35°. This is a substantiation of the accuracy of the system when the antenna pattern is immersed in a uniform medium. Snow also has an apparent temperature close to ambient but water is considerably colder.

TABLE 3. Average Temperature as a Function of Terrain and Elevation Angle

Elevation Angle	-35°	-5°
Over-Land Average Temp	$263^{\circ}K$	$182^{\circ}K$
Over-Water Average Temp	$90^{\circ}K$	$63^{\circ}K$
Over-Snow Average Temp	$237^{\circ}K$	$153^{\circ}K$

This table implies that snow and land may be considered similar to blackbodies when observed at low elevation angles. Water, however, displays the expected characteristic of a partial reflector.

On the basis of these tests and considerations:

(1) Over-water, over-land, and over-snow curves shown in Figure 7 demonstrate the effects of sidelobe leakage from ground environments; that is, the disparities shown do not indicate actual differences in sky temperature over different ground environments but they rather indicate the differences in the equivalent temperatures of the ground environments themselves. This will be one of the major problems

in designing a sensitive airborne X-band communications system, especially if antenna elevation angles close to the horizon are desired.

(2) Due to the low observed temperatures of water, the over-water measurement of sky temperature is least influenced by antenna sidelobe contributions. Therefore the over-water average plot, Curve C of Figure 7, presents the lowest observed temperatures, and is taken to be the upper bound of sky noise contribution for clear weather conditions.

(3) Considering the fact that the over-water average temperature curve has no correction for sidelobe leakage, although the energy entering the sidelobes from the water is low, and that observed over-water temperature approaches zero at elevation angles near 70° (Table 3), the sky temperature calculated by Boeing (see footnote, p. 9) seems reasonable, at least at 35,000 ft. The Boeing report contains a derivation of sky noise temperature as a function of elevation angle for various aircraft altitudes. The comparison of the Boeing curve against the over-water average is shown in Figure 7.

(4) Land and snow approximate blackbody radiators at ambient atmospheric temperature at the measurement frequency. At observation angles below the horizontal, water appears to approximate a partially reflective surface.

(5) Altitude elevation profiles show a barely noticeable trend toward decreasing sky noise temperature as a function of increasing altitude. Note that no attempt has been made to remove sidelobe leakage from these measurements. Sidelobe pickup undoubtedly is the cause of the large altitude effect at near-horizontal elevation angles.

Appendix A

System Operation

A block diagram of the system is shown in Figure 1, page 2. This type of radiometer operates in the comparison mode in a straightforward manner. The ferrite switch alternately samples the output of the directional coupler and the noise from a room temperature reference termination. If the average noise output from the directional coupler is different from that of the reference load, there will be a noise input to the mixer-preamplifier which fluctuates at (or is modulated by) the sampling frequency. This input to the mixer-preamplifier is mixed down to a 30 Mcps IF frequency by the klystron local oscillator. The IF signal is amplified and video detected and then passed through a filter resonant at the sampling frequency. The filter output (which approaches a sine wave) is amplified and detected synchronously with the sampling frequency. The resultant signal is a fluctuating dc voltage that is smoothed by integration and applied to a zero-center meter.

If the directional-coupler output is greater than that of the reference load, the synchronously detected dc voltage will be of one polarity. If the reference load output is greater than the coupler output, the synchronously detected dc output will be of the opposite polarity.

If the coupler output is equal to the reference load noise output, there will be no sampling-frequency-modulated input to the mixer preamplifier, and thus no output at the meter; that is, the meter will read 0. This condition of equality or null

balance is obtained if the sum of antenna entrant noise through the coupler loss, the energy from the noise source through its attenuator, and the loss in the coupler equals the energy out of the reference load. This condition is obtained by adjustment of the attenuator between the noise source and the coupler. Assuming that the system has been calibrated, the attenuator reading may be used to define the magnitude of antenna-entrant (or source) noise equivalent blackbody temperature.

System operation is extremely simple. The attenuator is adjusted to produce a 0 output at the meter. The attenuator reading is chart-converted to equivalent source temperature. If the ambient room temperature fluctuates, its value is noted and applied as a correction. Antenna elevation angle is also monitored on a meter. Aircraft skin temperature (for data conversion purposes), heading, and ground position are also noted. External meteorological and ground environment conditions are monitored visually through an observation window. Aircraft bank angle is defined by the pilot.

NOTES ON RADIOMETER CALIBRATION

For a radiometer with a room temperature reference, T_o, and an injection noise source, TN, of equivalent temperature such that

$$TN >> T_o, \tag{1}$$

a calibration equation may be derived which depends only on the accuracy of the relative change in loss of the attenuator in the noise source arm of the device. This equation implies radiometer calibration over the entire range with one calibration point.

Consider the radiometer front end shown below

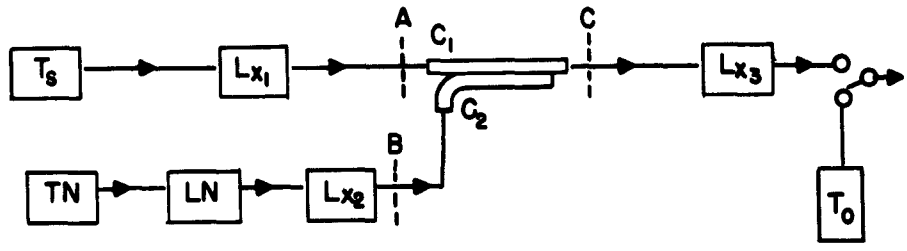

Figure 13. Radiometer Calibration

where

T_s = calibration source

TN = noise source, $TN >> T_o$

T_o = room temperature reference

$L_{x_{1,2,3}}$ = unknown losses to T_o

C_1, C_2 = directional coupler coefficients

LN = precision attenuator

The temperature entering the coupler at A is

$$T_A = \frac{T_s}{L_{x_1}} + \frac{L_{x_1} - 1}{L_{x_1}} T_o \tag{2}$$

and at B

$$T_B = \left(\frac{TN}{LN} + \frac{LN-1}{LN} T_o\right)\frac{1}{L_{x_2}} + \frac{L_{x_2} - 1}{L_{x_2}} T_o \tag{3}$$

$$= \frac{TN}{LNL_{x_2}} + \frac{LNL_{x_2} - 1}{LNL_{x_2}} T_o \ .$$

T_C, the temperature exiting the coupler at C, is

$$T_C = C_1 T_A + C_2 T_B$$

$$= C_2 (T_B - T_A) + T_A , \tag{4}$$

since

$$C_1 + C_2 = 1 . \tag{5}$$

For equal energy at each switch port

$$\frac{T_C}{L_{x_3}} + \frac{L_{x_3} - 1}{L_{x_3}} T_o = T_o . \tag{6}$$

Thus

$$T_C = T_o . \tag{7}$$

Equations (2), (3), and (7), when incorporated into Eq. (4), yield

$$T_C = T_o = C_2 \left\{ \left[\frac{TN}{LNL_{x_2}} - \frac{T_s}{L_{x_1}} \right] + T_o \left[\frac{LNL_{x_2}{}^{-1}}{LNL_{x_2}} - \frac{L_{x_1}{}^{-1}}{L_{x_1}} \right] \right\} + \frac{T_s}{L_{x_1}} + \frac{L_{x_1}{}^{-1}}{L_{x_1}} T_o . \tag{8}$$

Simplification produces

$$T_s = \frac{T_o L_{x_1}}{(1-C_2)} \left[C_2 \left(\frac{L_{x_1}{}^{-1}}{L_{x_1}} - \frac{LNL_{x_2}{}^{-1}}{LNL_{x_2}} \right) + \frac{1}{L_{x_1}} \right] - \frac{TNC_2 L_{x_1}}{(1-C_2) LNL_{x_2}}$$

$$= \frac{T_o L_{x_1}}{(1-C_2)} \left[\frac{1}{L_{x_1}} (1-C_2) \right] + \frac{T_o L_{x_1}}{(1-C_2)} \left[C_2 \left(1 - \frac{LNL_{x_2}{}^{-1}}{LNL_{x_2}} \right) \right] - \frac{TNC_2 L_{x_1}}{(1-C_2) LNL_{x_2}}$$

$$= T_o - \frac{1}{LN} \left[\frac{C_2 L_{x_1}}{(1-C_2) L_{x_2}} \right] \left[TN - T_o \right]$$

$$= T_o - \frac{K}{LN} \left[TN - T_o \right] , \tag{9}$$

where

$$K = \frac{C_2}{(1-C_2)} \left(\frac{L_{x_1}}{L_{x_2}} \right) = \left(\frac{C_2}{C_1} \right) \left(\frac{L_{x_1}}{L_{x_2}} \right) . \tag{10}$$

Thus, at $T_s = T_{s_1}$, a known temperature,

$$K = \frac{LN\left(T_o - T_{s_1}\right)}{(TN - T_o)} . \tag{11}$$

Equation (9) may be used to derive radiometer calibration curves for various room temperatures, provided $K/LN << \Delta T_{min}$, minimum incremental sensitivity.

Appendix B

Data Reduction Method

At the conclusion of data flights, the antenna, enclosure, and radome were removed from the aircraft and tested on an antenna range to determine VSWR, radome loss, and pattern dispersion. The determination of VSWR, radome loss, and their meaningfulness in data reduction are outlined in the following deriyation.

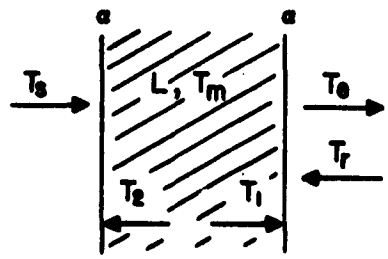

Figure 14. Bounded Lossy Medium

Consider Figure 14 a bounded lossy medium at equilibrium temperature T_m. Assume medium loss from inner boundary to inner boundary horizontally to be L. Assume external noise energies equivalent to T_s and T_r to be incident as shown. Assume the power reflection coefficient at each interface to be α.

T_e, the equivalent temperature radiated to the right, may be expressed:

$$T_e = f(T_s, T_m, T_r, L, \alpha). \tag{1}$$

For convenience let T_1 and T_2 be introduced from thermodynamic considerations where

$$T_1 = \frac{L-1}{L} T_m + T_s \frac{(1-\alpha)}{L}, \tag{2}$$

$$T_2 = \frac{L-1}{L} T_m + T_r \frac{(1-\alpha)}{L}. \tag{3}$$

Rewriting Eq. (1),

$$\begin{aligned} T_e &= g(T_1, T_2) + \alpha T_r \\ &= g(T_1, 0) + g(0, T_2) + \alpha T_r. \end{aligned} \tag{4}$$

Now

$$\begin{aligned} g(T_1, 0) &= T_1(1-\alpha) + \left(\frac{\alpha}{L}\right)^2 T_1 (1-\alpha) + \left(\frac{\alpha}{L}\right)^4 T_1 (1-\alpha) + \ldots \\ &= T_1(1-\alpha) \sum_{n=0}^{\infty} \left(\frac{\alpha}{L}\right)^{2n} \\ &= T_1 \frac{L^2(1-\alpha)}{L^2-\alpha^2}, \end{aligned} \tag{5}$$

and

$$\begin{aligned} g(0, T_2) &= T_2 \frac{\alpha}{L} (1-\alpha) + T_2 \left(\frac{\alpha}{L}\right)^3 (1-\alpha) + \ldots \\ &= T_2 \frac{\alpha}{L}(1-\alpha) \sum_{n=0}^{\infty} \left(\frac{\alpha}{L}\right)^{2n} \\ &= T_2 \frac{\alpha L(1-\alpha)}{L^2-\alpha^2}. \end{aligned} \tag{6}$$

Substitution in Eq. (4) of Eqs. (5) and (6) yields

$$T_e = (T_1 L + T_2 \alpha) \frac{L(1-\alpha)}{L^2-\alpha^2} + \alpha T_r$$

$$= T_m \frac{(L-1)(L+\alpha)(1-\alpha)}{L^2-\alpha^2}$$

$$+ T_s \frac{L(1-\alpha)^2}{L^2-\alpha^2}$$

$$+ T_r \left[\frac{\alpha(1-\alpha)^2}{L^2-\alpha^2} + \alpha \right] . \tag{7}$$

Rewriting T_r,

$$T_r = T_m + (T_r - T_m), \tag{8}$$

and substituting in Eq. (7)

$$T_e = T_m - \frac{L(1-\alpha)^2}{L^2-\alpha^2} \left[T_m - T_s \right] + (T_r - T_m) \left[\frac{\alpha(1-\alpha)^2}{L^2-\alpha^2} + \alpha \right] . \tag{9}$$

Consider conditions for which

$$T_r >> T_m, \ T_s . \tag{10}$$

Then, from Eq. (9)

$$T_e \cong T_r \left[\frac{\alpha(1-\alpha)^2}{L^2-\alpha^2} + \alpha \right]$$

$$\cong K^2 T_r . \tag{11}$$

Equation (9) may now be rewritten

$$T_e = T_m - \frac{1}{L'} \left[T_m - T_s \right] + K^2 \left[T_r - T_m \right], \tag{12}$$

where

$$L' = \frac{L^2-\alpha^2}{L(1-\alpha)^2}, \tag{13}$$

and

$$K^2 = \alpha \left[1 + \frac{(1-\alpha)^2}{L^2-\alpha^2} \right] = \alpha \left[1 + \frac{1}{LL'} \right] . \tag{14}$$

For the purpose of a first-order approximation to the antenna-enclosure-radome contributions, the following assumptions were made:

a. Let T_e be recorded data temperature
b. Let T_s be external noise temperature
c. Let $T_m = T_w$, the average radome temperature
d. Let $T_r = T_o$, the radiometer thermodynamic load reradiation
e. Let K^2 be defined as the power reflection corresponding to measured VSWR
f. Let L' be the radome loss corrected for radome boundary reflections
g. Assume L' constant across main beam and equal to 1 over the remainder of the pattern

K^2 was obtained from VSWR measurements. L' was obtained by zenith measurements, assuming $T_r = T_m$, and $T_s << T_m$. These tests were conducted on an antenna range using antenna, enclosure, radome, and simulated aircraft skin.

On the basis of the above assumptions, Eq. (14) was rewritten as

$$T_s' = T_w - L' \left\{ \left[T_w - T_e \right] + K^2 \left[T_o - T_w \right] \right\}, \tag{15}$$

where T_s' represents the external noise temperature in the pattern sidelobes as well as the main beam.

Equation (15) was used for data reduction.

Appendix C

Antenna Considerations

The schedule for construction and installation of the antenna enclosure and radome in the aircraft, and the tight schedule of the airborne data-gathering program, prohibited pattern testing of the antenna-enclosure-radome complex until after completion of the airborne work. Thus, except for the free-space pattern of the antenna alone, all pattern measurements and derivations pertinent to the antenna-enclosure-radome complex were initiated upon completion of airborne data gathering.

In considering the antenna patterns presented in this appendix, the E-plane pattern corresponds to the elevation pattern and the H-plane pattern to the azimuth pattern. The patterns of Figures 15 through 18 were taken on an antenna range. The antenna-enclosure-radome unit was removed from the aircraft and installed on the range. An equivalent aircraft skin was fabricated to duplicate airborne electrical surface conditions in the vicinity of the radome. No enclosure shielding was necessary because the enclosure itself was constructed of aluminum.

Figures 15a and 15b represent E- and H-plane patterns of the 1-ft antenna in free space. Consideration of these patterns and the predicted slot effects of the enclosure led to the choice of horizontal polarization to minimize H-plane (azimuthal) sidelobes.

Figures 16a and 16b are elevation (E-plane) and azimuth (H-plane) patterns of the antenna within the enclosure with radome installed, taken at a representative

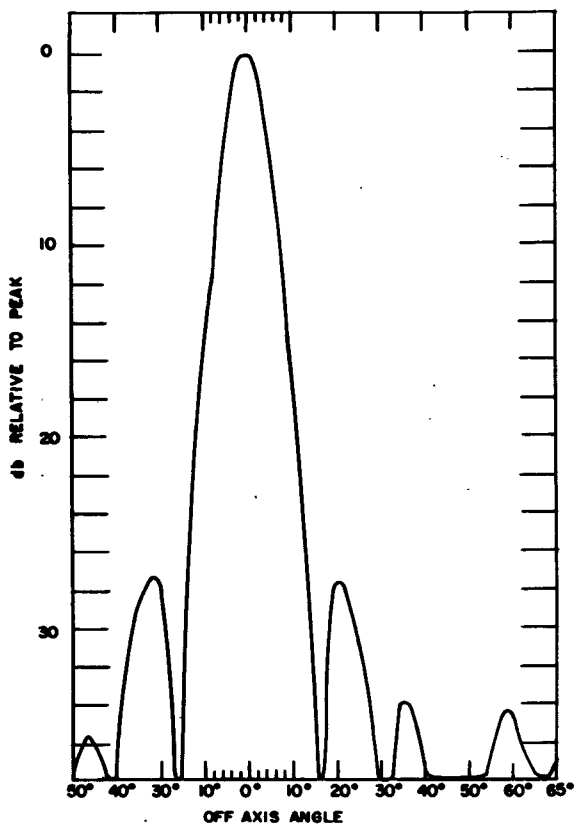

Figure 15a. E-Plane Free-Space Pattern 1-ft Dish, f = 8030 Mcps

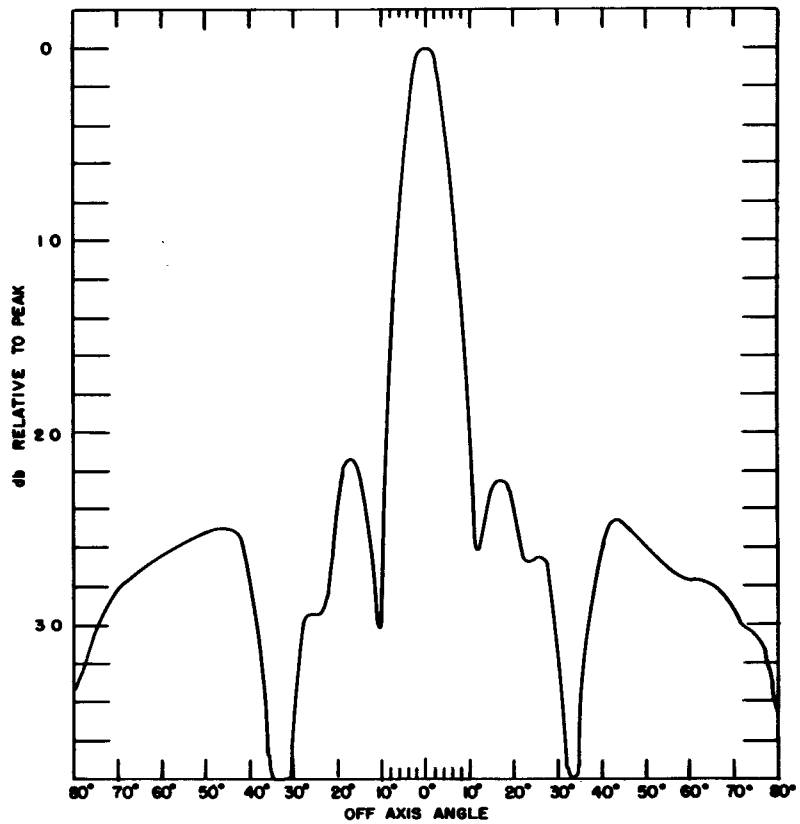

Figure 15b. H-Plane Free-Space Pattern 1-ft Dish, f = 8030 Mcps

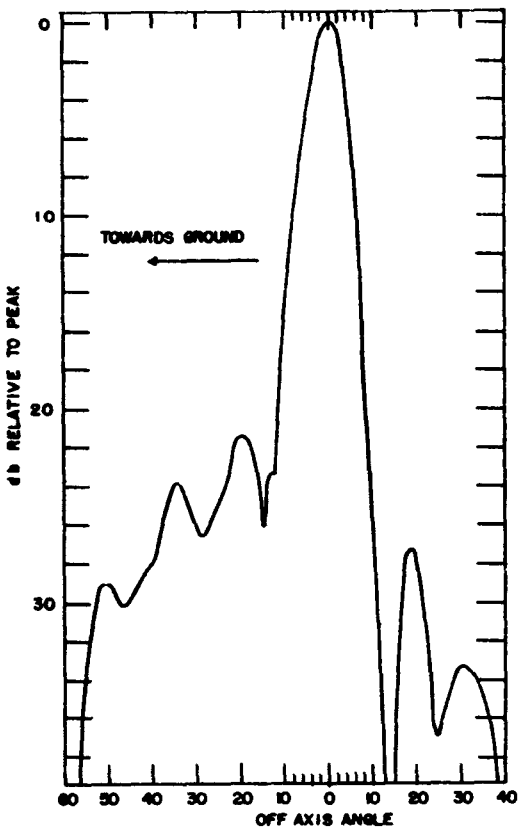

Figure 16a. Elevation (E Plane) Pattern of 1-ft Antenna in Enclosure with Radome. Antenna elevation angle within enclosure equals 20° with respect to aircraft horizontal. f = 8030 Mcps.

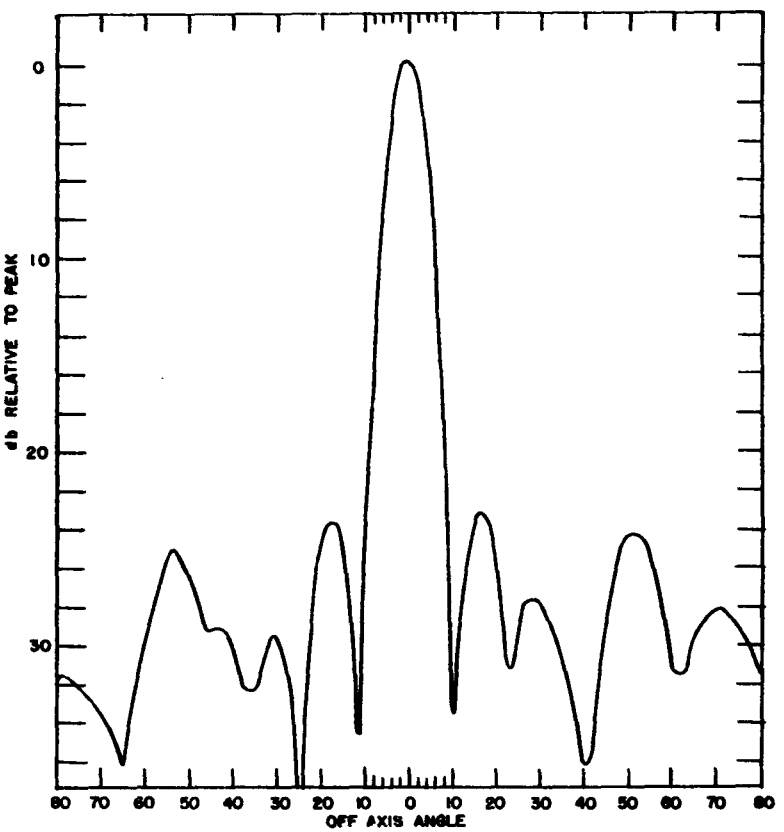

Figure 16b. Azimuth (H Plane) Pattern of 1-ft Antenna in Enclosure with Radome. Antenna elevation angle within enclosure equals 20° with respect to aircraft horizontal. f = 8030 Mcps.

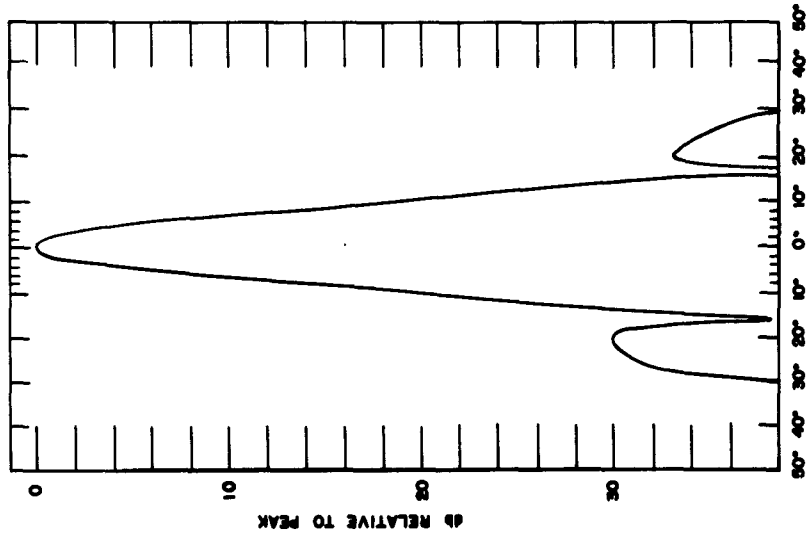

Figure 17. Elevation Pattern (E Plane) of 1-ft Antenna in Enclosure without Radome. Antenna elevation angle within enclosure equals 10°.

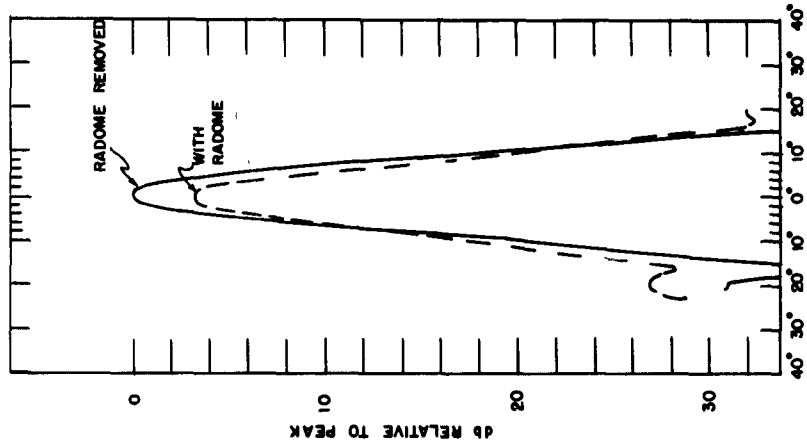

Figure 18. Elevation (E Plane) Patterns of 1-ft Antenna within Enclosure with and without Radome. Antenna elevation angle within enclosure equals 10°.

antenna elevation angle ($+20^{o}$ with respect to aircraft horizontal). Comparison with Figures 15a and 15b shows sidelobe enhancement in the E-plane and suppression in the H-plane. Also note the reduction in the H-plane beamwidth.

Figure 17 represents an elevation (E-plane) pattern (antenna elevation = $+10^{o}$) with the radome removed. Comparison with Figures 15a and 15b indicates that the radome is the major source of sidelobe enhancement and beam distortion in the elevation pattern. Figure 18 shows the elevation pattern main-beam gain difference at an antenna elevation angle of $+10^{o}$ with and without the radome. One db of the difference can be attributed to radome loss and power reflection (L' in Appendix B). The remaining 2 db difference is taken to be a measure of beam broadening and sidelobe enhancement arising from radome-caused redistribution of energy in the pattern.

E-plane (elevation) main-beam broadening and sidelobe enhancement permit considerable temperature contributions from ground that is below the main beam of the antenna. Rough calculations based on these antenna patterns appear to explain the deviation of observed over-land and over-snow average temperatures from the over-water temperatures. Assuming ground-temperature-equivalent blackbody radiation from land and snow, these calculations have yielded 'corrected' over-land and over-snow averages within 20 percent of the over-water values. However, since the antenna patterns are far from being completely documented and since water is not a blackbody, in presenting the results of this experiment no attempt has been made to correct the data other than for the radome loss and reflection.

AF Cambridge Research Laboratories, Bedford, Mass. Electronics Research Directorate
HIGH ALTITUDE X-BAND NOISE MEASUREMENTS by S. Hunt, A. Orange and K. Glick. April 1963. 31 pp. incl. illus. AFCRL-63-87

Unclassified report

X-band noise temperature data obtained with an airborne radiometer installed in a high-speed jet aircraft (KC-135) is presented. The aircraft was found to be an electrically quiet environment at X-band. The data shows the considerable influence of blackbody radiation from the earth entering the antenna sidelobes. Temperatures close to those calculated theoretically were measured over water and at high antenna elevation angles. Heavy clouds, though many thousands of feet below the aircraft, caused a considerable temperature increase. A trend of lower temperatures with increasing altitude was observed. The apparent temperatures of land, snow, and ice and water is discussed.

UNCLASSIFIED

1. Microwave Communications Systems
2. Radio Transmission
3. Electromagnetic Absorption (in atmosphere)

I. Hunt, S.
II. Orange, A.
III. Glick, K.

UNCLASSIFIED

AF Cambridge Research Laboratories, Bedford, Mass. Electronics Research Directorate.
HIGH ALTITUDE X-BAND NOISE MEASUREMENTS by S. Hunt, A. Orange and K. Glick. April 1963. 31 pp. incl. illus. AFCRL-63-87

Unclassified report

X-band noise temperature data obtained with an airborne radiometer installed in a high-speed jet aircraft (KC-135) is presented. The aircraft was found to be an electrically quiet environment at X-band. The data shows the considerable influence of blackbody radiation from the earth entering the antenna sidelobes. Temperatures close to those calculated theoretically were measured over water and at high antenna elevation angles. Heavy clouds, though many thousands of feet below the aircraft, caused a considerable temperature increase. A trend of lower temperatures with increasing altitude was observed. The apparent temperatures of land, snow, and ice and water is discussed.

UNCLASSIFIED

1. Microwave Communications Systems
2. Radio Transmission
3. Electromagnetic Absorption (in atmosphere)

I. Hunt, S.
II. Orange, A.
III. Glick, K.

UNCLASSIFIED

AF Cambridge Research Laboratories, Bedford, Mass. Electronics Research Directorate
HIGH ALTITUDE X-BAND NOISE MEASUREMENTS by S. Hunt, A. Orange and K. Glick. April 1963. 31 pp. incl. illus. AFCRL-63-87

Unclassified report

X-band noise temperature data obtained with an airborne radiometer installed in a high-speed jet aircraft (KC-135) is presented. The aircraft was found to be an electrically quiet environment at X-band. The data shows the considerable influence of blackbody radiation from the earth entering the antenna sidelobes. Temperatures close to those calculated theoretically were measured over water and at high antenna elevation angles. Heavy clouds, though many thousands of feet below the aircraft, caused a considerable temperature increase. A trend of lower temperatures with increasing altitude was observed. The apparent temperatures of land, snow, and ice and water is discussed.

UNCLASSIFIED

1. Microwave Communications Systems
2. Radio Transmission
3. Electromagnetic Absorption (in atmosphere)

I. Hunt, S.
II. Orange, A.
III. Glick, K.

UNCLASSIFIED

AF Cambridge Research Laboratories, Bedford, Mass. Electronics Research Directorate
HIGH ALTITUDE X-BAND NOISE MEASUREMENTS by S. Hunt, A. Orange and K. Glick. April 1963. 31 pp. incl. illus. AFCRL-63-87

Unclassified report

X-band noise temperature data obtained with an airborne radiometer installed in a high-speed jet aircraft (KC-135) is presented. The aircraft was found to be an electrically quiet environment at X-band. The data shows the considerable influence of blackbody radiation from the earth entering the antenna sidelobes. Temperatures close to those calculated theoretically were measured over water and at high antenna elevation angles. Heavy clouds, though many thousands of feet below the aircraft, caused a considerable temperature increase. A trend of lower temperatures with increasing altitude was observed. The apparent temperatures of land, snow, and ice and water is discussed.

UNCLASSIFIED

1. Microwave Communications Systems
2. Radio Transmission
3. Electromagnetic Absorption (in atmosphere)

I. Hunt, S.
II. Orange, A.
III. Glick, K.

UNCLASSIFIED